A Novel Bi-directional Grid Inverter Control Based on Virtual Impedance Using Neural Network for Dynamics Improvement in Microgrids

Mohamad Alzayed, *Member, IEEE*, Michel Lemaire, Hicham Chaoui, *Senior member, IEEE*, and Daniel Massicotte, *Senior member, IEEE*

***Abstract*—In microgrids, the voltage source inverters often use the droop control technique along with voltage and inner current control loops to achieve a reliable electrical supply. Because of the unmatched line impedance, the standard droop control technique makes it difficult to uniformly distribute power and limit circulating flow across parallel connections, especially in highly nonlinear systems. The purpose of this research is to introduce a neural network-based virtual impedance integrated with a bi-directional grid inverter control technique that improves stability during the dynamic operation of microgrids. In order to track demand and reference power accurately with less deviation and better stability under various operating scenarios, the suggested technique employs the Feed-Forward Neural Network (FFNN) to learn the nonlinear model during the transient state of the inverter. It consists of adding compensation voltages without any further tuning procedure. The proposed FFNN controller's extensive transient stability analysis, power tracking, and operational performance are assessed in various dynamic scenarios using the power hardware-in-the-loop (PHIL) technique. In addition, the robustness and performance of the proposed approach are validated on the IEEE 33-bus standard distribution system. All findings are compared to the tried-and-true conventional technique to demonstrate its efficacy.**

***Index Terms*—feed-forward neural network, inverter-based power system, virtual impedance, microgrid, droop control.**

I. Introduction

THE concept of microgrids which are integrated with distributed energy resources (DERs), has been utilized commonly in recent years due to the devastating environmental effects of classical power generation stations into power grids and the growing worldwide need for decarbonizing energy [1], [2]. Distributed generation (DG) systems that can provide electricity in both off-grid (islanded) and grid-connected (GC) functioning modes have been made possible because of developing technologies, advances, and enhanced control in power converter/inverter systems [3].

M. Alzayed, M. Lemaire, and D. Massicotte are with the Laboratory of Signal and System Integration (LSSI), Department of Electrical and Computer Engineering, Université du Québec à Trois-Rivières, Trois-Rivières, QC, G9A 5H7, Canada. (e-mail: mohamad.alzayed@uqtr.ca; michel.lemaire1@uqtr.ca; daniel.massicotte@uqtr.ca).
M. Alzayed and H. Chaoui are with Intelligent Robotic and Energy Systems Research Group (IRES), Department of Electronics, Carleton University, Ottawa, ON, K1S 5B6, Canada. (e-mail: mohamad.alzayed@carleton.ca; hicham.chaoui@carleton.ca).

This work has been funded by the Natural Sciences and Engineering Research Council of Canada grant, Prompt, Opal-RT, Hydro-Québec, Canada Foundation for Innovation, CMC Microsystems, and the Research Chair on Signal and intelligent high-performance systems.

Droop control techniques are among the strategies that assist in controlling the interchange of shared power in inverter-based microgrids, and their importance has recently grown [4]–[6]. The droop controller is the main device that is frequently used in grid inverters/converters to increase the stabilization of microgrids [7]. Reactive power-voltage magnitude droop control and active power-frequency droop control are the two main operating principles for typical conventional droop-controlled inverters. The droop control is become more popular as a result of its benefits, including simple installation, adaptive parameter adjustment, active and reactive power adjustment in the absence of DERs' data connection, and a significant level of dependability [7]–[9]. In contrast, the standard droop control system has significant drawbacks and shortcomings, including frequency and/or voltage variations, DGs' system transient behavior impact, a drop of inertia assistance in mega inverter-based grids during dynamic operation, inaccuracies in delivered power value with variable coupling impedance, and instability states due to insufficient dynamic action [10]–[13].

Conventional droop controllers function poorly when applied to grids with unknown line compensations, transmission lines with complex impedance, or distribution systems that are primarily resistive. Additionally, the impedance mismatch at the terminals of side-by-side inverters has a negative effect on droop controllers. Otherwise, the synchronized virtual impedance is formulated using a complex virtual impedance that incorporates both inductance and resistance elements. These components, inductance and resistance, are utilized to offset discrepancies in reactive and active power, respectively. By concurrently adjusting virtual resistance and virtual inductance, the compensation is extended to address incongruities in line impedance among DGs. This dual-tuning approach not only ensures accurate power sharing but also contributes to bolstering the overall stability of the microgrid system by augmenting damping across the entire system [14]. As a result, these circumstances lead to uneven power distribution and, ultimately, instability. Since the correct frequency and voltage regulation in microgrids and accurate active and reactive power-sharing capabilities are both essential for converter-controlled distributed generators, many adjusted droop control structures are developed to tackle this problem. In [15]–[18], the concept of virtual impedance is implemented. An optimal adjustment of complex virtual impedance is adopted for each inverter to enhance power-sharing accuracy by calculating feeder impedance using an online estimation algorithm

[15]. In [16], authors propose an adaptive virtual impedance controller for reconfigurable AC/DC MicroGrids that enables autonomous adaptation of output impedance of inverters to ensure power sharing enhancement. It is noteworthy that the virtual impedance concept can be deployed to ameliorate power quality by compensating harmonic power sharing while supplying nonlinear loads [17].

The aforementioned systems have certain drawbacks, including a lack of precise active and reactive power decoupling, dependence on the structure of microgrids, and a need for more measurement instruments. Therefore, several current methods seek to improve the droop controllers even further through intelligent control methods [19]–[22]. For the purpose of load-shedding and power sharing in a droop-controlled islanded microgrid, the authors in [19] present a probabilistic wavelet fuzzy neural network technique to take the place of the voltage regulator, which is based on a PI controller. Even yet, the method has a long execution time, and its deployment is limited to microgrids powered by battery energy storage. For the enhancement of power-sharing in microgrid systems, a hierarchical control framework based on radial basis function neural networks (RBFNN) is adopted in [23]. In this approach, a basic PI-based voltage control loop is added to the multilevel control scheme, using the PIRBFNN methodology to solve power flow equations and obtain reactive power references. As a result, the low-pass filter in the droop control system is no longer required. But since the new PI controller must be properly tuned in order for this technique to be accurate, the system becomes more complicated. Moreover, it does not include any physical application of the presented strategy or give evidence of the offered method's accuracy in reactive power-sharing. In [21], a reinforcement learning-based data-driven intelligent control is provided for customizing the settings of virtual inertia emulation for frequency control. As opposed to power-sharing capabilities, the frequency management of microgrids is the major topic of this work. This technique is a model-based strategy that necessitates knowledge of the system model beforehand. For voltage and frequency stabilization and power-sharing control, the authors in [22] suggest a data-driven online learning method to take over the traditional droop control technique. The method's limitation is that reactive power sharing must take precedence over greater voltage faults in order to achieve both voltage control and reactive power sharing concurrently. To address the constraints of tuning back-to-back PI regulators, separate tuning for various system sizes, and the calculation complexity of the other methods, the cascade-forward neural network (CFNN) approach to driving inverter-based grids is presented in [24]. The CFNN system gains benefit from the online weights adaptation technique by following the nominal system voltage and frequency, or active and reactive power, in islanded/grid-connected mode, respectively. Otherwise, this CFNN technique exhibits some divergence during the dynamic transition.

The feed-forward neural network (FFNN) trained using the back-propagation algorithm, as opposed to the most straightforward (PI controller) and widely used systems, is recommended in contrast to the prior approaches. The advantage of the FFNN is that it can handle nonlinear connections between input and output while maintaining a linear relationship. Besides, to follow the reference parameters based on the operational mode, a live neuron-weight modification algorithm is used to drive the feedback signals to zero. In the context of our application, the advantage of applied FFNN is not only its inherent ability to handle non-linear relationships but also its flexibility in managing linearity. The used FFNN architecture allows for a more controlled and interpretable adjustment of its parameters, making it feasible to introduce linear components when needed. This flexibility can be advantageous in scenarios where preserving or incorporating linear characteristics is beneficial for specific aspects of the control strategy. Also, the conventional modeling and standard virtual impedance control may be effective in many scenarios, while neural networks can offer advantages in situations where the system dynamics are complex, non-linear, or subject to uncertainties that are challenging to model accurately. Accordingly, the FFNN virtual impedance technique is suggested with minimal oscillation during dynamic operation, such as a fault or transition state, to address the other methods' limitations of: i) single tuning for various system sizes and/or installation locations; ii) the conventional method's unstable condition in highly nonlinear cases; iii) the complexity of the adaptation in the other common techniques. The proposed approach is unit-based, making it general enough to be applied to a variety of converter-controlled distributed generator sizes without extra tuning. By monitoring the reference and actual currents in islanded or grid-connected mode, the live weights adaption technique adds value to the suggested system and results in less oscillation during dynamic operating conditions such as faults or transition states.

In brief, the contribution of the paper is:

- Introducing a virtual impedance-based universal FFNN to enhance inverter-based microgrids with bi-directional islanded/grid-connected modes control.
- The feedback errors are driven to zero by online neural network neuron-weight adaptation, which makes it simpler for the suggested technique to monitor the reference values to increase system stability, less oscillation.
- The FFNN virtual impedance technique gets around the limitations of single tuning for various system sizes and/or installation locations, the conventional method's unstable condition in highly nonlinear cases, and the complexity of the adaptation in the other common techniques.
- Multiple PHIL experimental assessments on 1MW BESSs using the IEEE 33-bus standard distribution system and real-time platform coupled with processor demonstrate the efficacy of the proposed approach. As a result, the offered scheme is verified and contrasted with the conventional supported method, revealing the effectiveness and robustness of the suggested strategy in the operating modes of islanded, grid-connected, and dynamic (fault/transition).

Section II analyzes the droop control and conventional virtual impedance concepts in microgrids. The proposed FFNN virtual impedance is executed for grid-supporting VSIs in

Section III. Besides, in Section IV, a transient stability analysis is conducted to prove the robustness of the proposed technique. The PHIL experimental results for the proposed and conventional methods are presented in Section V, as well as the IEEE 33-bus standard test in Section VI. Section VII wraps up the research with a comprehensive overview and a detailed conclusion.

II. Virtual Impedance Theory in Microgrids

Fig. 1. Three-phase VSI with LC filter circuit layout.

Voltage Source Inverters (VSI) are utilized in modern utilities to incorporate both battery energy storage devices and distributed power sources. Therefore, an LC filter, which is regarded as an interface device, is used to connect the VSI to the grid. The power source, VSI, LC filter, and grid-connected impedance are shown in Fig. 1. The LC filter consists of L_s, R_s at the VSI side and parallel capacitor C_f, and Lg, Rg at the grid connection point. v_i^{abc} and i_i^{abc} are the VSI 3-phase voltage and current, and v_g^{abc} and i_g^{abc} the grid or load side voltage and current. Also, v_o^{abc} is the filter's tie-point voltage. A droop, along with current and voltage control loops, make up the traditional control framework for VSI-based microgrids. The mathematical control model is constructed using the conventional control approach described in [7] as a benchmark model.

A. Droop Control model

A primary-level controller known as a "droop controller" is used in microgrids to regulate the output power (P, Q) using the frequency and amplitude of the inverter's terminal voltage. The algorithm for conventional droop control is developed as follows [24],

$$\omega = \omega_o + m_p(P^{ref} \quad P^{act}) \tag{1a}$$

$$E = E_o + m_q(Q^{ref} \quad Q^{act}) \tag{1b}$$

where E and ω are the amplitude and angular frequency of the inverter's terminal signal, E_o and ω_o are the reference or nominal values of voltage amplitude and angular frequency, m_q and m_p are the droop controller gains, P^{ref} and Q^{ref} are active and reactive reference power values, and P^{act} and Q^{act} are the measured active and reactive power, respectively.

B. Current Regulator Control Loop

1) Islanded mode: The main function of the current control loop is to improve the voltage level of microgrids in IS operating mode. The voltage regulator block, which modifies the output voltage of the inverter, is part of the outer control loop. It is important to underline that the voltage regulation loop is only triggered in islanded operation. The voltage control loop's mathematical equations are expressed as,

$$i_d^{ref} = K_{p1}\ e_{v_d} + K_{i1} \int e_{v_d} \tag{2a}$$

$$i_q^{ref} = K_{p2}\ e_{v_q} + K_{i2} \int e_{v_q} \tag{2b}$$

where, $e_{v_d} = v_d^{ref} \quad v_{gd} = E \quad v_{gd}, e_{v_q} = 0 \quad v_{gq}, v_{gdq}$ is the dq-axis voltage at the grid-side, i_{dq}^{ref} is the reference current on dq-axis, $K_{p1,2}$ and $K_{i1,2}$ are the PI controllers' gains.

2) Grid connected mode: The primary objective revolves around the concept of distributing both active and reactive power within microgrids. This is achieved by implementing intricate control mechanisms that encompass inner/outer loops for voltage and current regulation. These control loops work harmoniously to ensure that the sharing of power is optimized and balanced, contributing to the efficient operation of the microgrid. This is accomplished by adjusting voltage amplitude and current in order to regulate the shared active and reactive power. The active power deviation is the driving signal of the PI controller in the active power control loop, whose output creates the d-axis reference current. The reactive power deviation is sent to the PI controller, and its output appoints the q-axis reference current, thus driving the reactive power control loop. Therefore, it is possible to derive the active and reactive power equations as,

$$i_d^{ref} = K_{p5}\ e_P + K_{i5} \int e_P \tag{3a}$$

$$i_q^{ref} = K_{p6}\ e_Q + K_{i6} \int e_Q \tag{3b}$$

where, $e_P = P^{ref} \quad P^{act}, e_Q = Q^{ref} \quad Q^{act}, K_{p5,6}$ and $K_{i5,6}$ are the PI controllers' gains.

C. Conventional Virtual Impedance

The voltage regulator control loop output voltages v_{dq} are written as (4),

$$v_d = v_{gd} + Ri_d^{ref} + L\frac{d}{dt}i_d^{ref} \quad \omega L i_q^{ref} \tag{4a}$$

$$v_q = v_{gq} + Ri_q^{ref} + L\frac{d}{dt}i_q^{ref} + \omega L i_d^{ref} \tag{4b}$$

where, $R = R_g$ and $L = L_g$.

The current regulator unit is the main component of the inner control loop, which serves as the inverter current regulator. The voltage loop combined with the current loop can be reconstructed from (4a) and (4b) as follows,

$$v_d = v_{gd} + Ri_d^{ref} \quad \overbrace{\omega L i_q^{ref}}^{\omega L_v i_d^{ref}} + K_{p3}\, e_{i_d} + K_{i3} \int e_{i_d} \tag{5a}$$

$$v_q = v_{gq} + Ri_q^{ref} + \overbrace{\omega L i_d^{ref}}^{\omega L_v i_q^{ref}} + K_{p4}\, e_{i_q} + K_{i4} \int e_{i_q} \tag{5b}$$

where, $e_{i_d} = i_d^{ref} \quad i_d$ and $e_{i_q} = i_q^{ref} \quad i_q$. $K_{p3,4}$ and $K_{i3,4}$ are the the PI controllers' gains. L_v is the Virtual impedance. Further, the controller desired voltage v_{dq}^* can be written as,

$$v_d^* = v_{gd} + Ri_d^{ref} \quad \omega L i_q^{ref} + v_d^+ \tag{6a}$$

$$v_q^* = v_{gq} + Ri_q^{ref} + \omega L i_d^{ref} + v_q^+ \tag{6b}$$

where in the conventional control system, v_{dq}^+ can be described as follows,

$$v_d^+ = \omega L_v i_d^{ref} = K_{p3}\, e_{i_d} + K_{i3} \int e_{i_d} \tag{7a}$$

$$v_q^+ = \omega L_v i_q^{ref} = K_{p4}\, e_{i_q} + K_{i4} \int e_{i_q} \tag{7b}$$

The inverter output impedance, virtual impedance, and feeder impedance are all included in the total output impedance. The key portion of the overall output impedance that influences system stability and dynamic performance is the inverter output impedance. The voltage and current control loop structures with decoupling elements are used to track the voltage reference precisely and quickly. The conventional PI regulator (5) is used in the voltage control loop ($\omega L_v i^{ref}$).

The characteristics of L_v are related to voltage stability. The gains should be tuned in such a way that the output voltage does precisely track the reference voltage. In fact, the line impedance in low-voltage microgrids is both resistive and inductive [18], making the separation of reactive and active power regulation challenging.

III. FFNN Virtual Impedance Inverter-Based Microgrid

A. Feed-Forward Neural Network Based Virtual Impedance

The control diagram of the FFNN virtual impedance-based bi-directional droop control approach that is proposed in this work is shown in Fig. 2. It contains a 3-phase voltage source inverter and an integrated conventional droop controller with FFNN virtual impedance for microgrid applications. The distributed generation units in the microgrid system cannot determine the relative amount of their line impedance, making it impossible to change the virtual impedance. To correct for line impedance mismatch, an FFNN-based virtual impedance control approach is presented. To satisfy the situation that the total output impedance is mainly inductive, the virtual inductance L_v must be regulated to regulate the actual current around its reference value. While the existing current controller addresses the immediate reference current requirements, the FFNN is designed to learn and adapt to more complex patterns and dynamic aspects of the system. Its goal is to predict and compensate for potential disturbances, uncertainties, or nonlinearities that may affect the system's performance.

Accordingly, the proposed FFNN-based virtual impedance aims to compensate for the drop voltage value and boosts the desired voltage to avoid any unstable situation during dynamic operation. The virtual impedance L_v is a function of the actual current (i^{act}), reference current (i^{ref}), and the deviation of these currents ($e_i = i^{ref} \quad i^{act}$).

For the grid inverter-based controller, extracting an accurate adaptive virtual impedance model requires understanding the link between the compensation voltage v_{dq}^+ and the load/reference current. The suggested model enhances the VSI's stability in grid-connected and islanded modes for microgrid applications. The neural network-implemented technique produces the compensating voltage v_{dq}^+ without using any of the standard virtual impedance (PI controller). This is able to be accomplished by creating the required dq-axes voltages to be added to the desired voltage in order to maintain stability.

The reference current i_{dq}^{ref} and actual current i_{dq}^{act} are used to identify the input signals for the FFNN. The proposed feed-forward neural network is trained to utilize an offline training approach using the data provided by the conventional virtual impedance model, a synthetic dataset (Section II-C). Feedback signals are required to reduce unexpected deviations caused by variations in the equivalent output impedance of the VSI and make up for the difference between the reference values and real values of the dq-axes currents. As a result, $e_{i_d} = i_d^{ref} \quad i_d^{act}$ and $e_{i_q} = i_q^{ref} \quad i_q^{act}$ determine the i_{dq}

Fig. 2. FFNN Virtual Impedance Bi-directional Inverter-Based Microgrid Control Block Diagram.

current feedback errors (ei). The strategy of live neuron-weights adaptation is employed to reduce these errors to zero. The suggested approach is unit-based, making it general enough to be applied to a variety of inverter-based system sizes without further tuning. The compensation voltage v_{dq}^{+} is added to the required voltage, as illustrated in Fig. 2.

B. Feed-Forward Neural Network

Fig. 3. Proposed Feed-Forward Neural Network scheme.

In systems where there is little understanding of the behavior, complexity, and dynamics of the system, neural networks are frequently used for estimation, modeling, and control. The parallelization and training capabilities of neural networks enable them to reach target values. The universal approximation theorem for neural networks states that they may properly estimate any nonlinear or dynamic properties [24]. The advantage of the FFNN is that it can handle nonlinear input-output interactions while maintaining a linear relationship. The following is a description of the relationship between the inputs and outputs of the FFNN.

$$\varphi_j^{(1)} = b_j^{(1)} + \sum_{i=1}^{m} w_{ji}^{(1)} x_i \tag{8a}$$

$$O_j^{(1)} = f_j^{(1)}(\varphi_j^{(1)}) \tag{8b}$$

$$\varphi_j^{(h)} = b_j^{(h)} + \sum_{p=1}^{h-1} \sum_{k=1}^{n} O_{jk}^{(p)} w_{jk}^{(p+1)} \tag{9a}$$

$$O_j^{(h)} = f_j^{(h)}(\varphi_j^{(h)}) \tag{9b}$$

where, x_i is the input signal for index i, m is the number of input signal, $w_{ji}^{(h)}$ is the weight of node j of layer (h) for input i, $b_j^{(h)}$ is the bias, $f_j^{(h)}$ is the activation function, and $O_j^{(h)}$ is the output signal. Layer index 1: 1^{st} hidden layer, h: h^{th} hidden layer , and o: output layer. n: number of neurons. Lastly, the FFNN output signals $\hat{y}$ can be declared as $\hat{y} = [y_1, y_2, .., y_l]$, where l is number of output signals.

Back-propagation learning is used to acquire the FFNN weight and bias parameters. The online weight adaptation law is also responsible for maintaining the robustness of the closed-loop control system as follows,

$$\hat{w}_{ji}^{(h)} = w_{ji}^{(h)} + e_i w_{ji}^{(h)} \tag{10a}$$

$$\hat{y} = f_l^{(o)}(b_l^{(o)} + \sum_{p=1}^{h-1} \sum_{k=1}^{n} O_{jk}^{(p)} \hat{w}_{jk}^{(p+1)}) \tag{10b}$$

where, $e_i = x_i^{ref} \quad x_i^{act}$, e_i is the feedback deviation/error of the input signal (i), x_i^{act} is the actual value of the neural network input signal, and x_i^{ref} is the reference value of the input signal (i).

As per Fig. 3, the suggested FFNN is made up of two layers. Ten neurons make up the input layer, 1^{st} layer, which is used to connect the input parameters (i.e., i_d^{ref}, i_d^{act}, i_q^{ref}, and i_q^{act}), and two neurons build up the output layer, 2^{nd} layer, (i.e.,v_d and v_q). The first and second layers are activated using the Purelin transfer function.

The suggested neural network's training data is generated using the conventional virtual impedance technique, a synthetic dataset. In this model, the ranges for the load's active power and reactive power are $[\ 1 \quad 1]pu$ and $[\ 0.7 \quad 0.8]pu$, respectively, in steps of 0.001 and 0.002. The learning data matrix is created using the conventional model findings in Section II-C. The mean square error (MSE) object of the test synthetic dataset, $MSE = \sum(yi \quad pi)^2/n$, is set at 0.0005, which represents half of the active power step, [24], [25]

Diverse scenarios where the microgrid is subjected to different grid conditions, transient events, and load variations are simulated. The correct value of the virtual impedance for system training is determined through a systematic process. Initially, comprehensive studies and simulations to assess the microgrid's performance under various virtual impedance settings are conducted. These simulations involve scenarios with changing grid conditions, transient events, and load fluctuations. To capture a wide range of operating conditions, the virtual impedance of the grid is intentionally varied during the training process. The Neural Network is exposed to scenarios with different virtual impedance values, allowing it to learn the system's responses and dynamics under varying impedance conditions. Through the extensive training process that includes a diverse set of scenarios, the FFNN learns to generalize and make predictions even in situations not explicitly encountered during training. Additionally, the live weights adaptation scheme plays a crucial role. The FFNN is continually updated based on real-time data, enabling it to adapt to unforeseen changes in operating conditions that may not have been explicitly covered during the training phase.

IV. Transient Stability Analysis

The active and reactive power of the DG presented in Fig. 1 can be expressed as follows:

$$P = \frac{v_o v_g}{x_o} \sin(\delta_o \quad \delta_g) = \frac{v_o v_g}{x_o} \sin(\delta) \tag{11a}$$

$$Q = v_g \frac{(v_o \quad v_g)}{x_o} \cos(\delta_o \quad \delta_g) = v_g \frac{(v_o \quad v_g)}{x_o} \cos(\delta) \tag{11b}$$

where, v_o and δ_o are the inverter tie-point voltage magnitude and phase angle, and v_g and δ_g are the grid/load side voltage magnitude and phase angle, respectively. Also, the power angle δ is the phase angle difference between the inverter side and grid side voltage. In addition, $x_o = x + x_v$, $L_o = L + L_v$, and the relationship of power angle δ and the angular velocity ω is derived as: $\omega = d\delta/dt$.

For the microgrid system during the transient state, even though the inverter-based grid is a second-order nonlinear system, determining its analytical solution makes it difficult to determine the transient stability. It is discovered that there is a structural similarity between the inverter-based grid nonlinear model and the swing equation of the synchronous generator. The inverter normally sends power to the load under normal operation, which demands that the power angle be no higher than , maximum boundary [26]. As a result, the drop in grid voltage and rise in line inductance are detrimental to the stability of synchronization. From (7) and (10), it is found that the virtual impedance is closely related to the PI parameters , , or , and the droop parameter . The negative damping/accelerating zone extends with a drop in and a rise in , , or in (1), which might result in the power inverter losing synchronization.

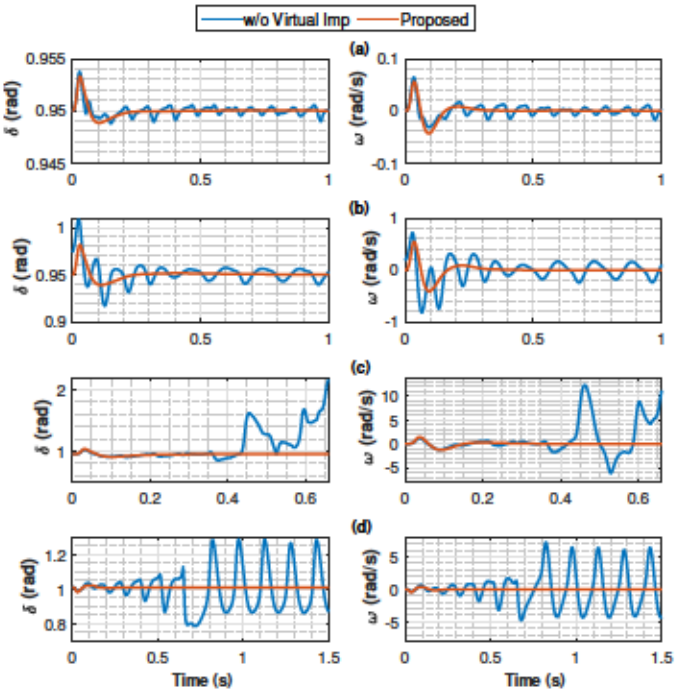

Fig. 4. Simulation results for power angle and angular velocity under: (a) small disturbance; (b) large disturbance; (c) fault disturbance; (d) grid transition disturbance.

According to [27], load switching, short circuits, or open circuits in AC transmission lines are the main causes of grid phase disruption. Also, authors in [28] present how grid failures can disturb the inverter's voltage phase. In reality, regardless of the type of large-signal disturbance (short circuit failure, load switching), the deviations in power angle and frequency demonstrate the system's stability performance. This section presents examples of transient responses to disturbances rather than a comprehensive stability analysis. The intent is to showcase the performance of the proposed approach under transient conditions (grid connection/disconnection, high renewable penetration, dynamic load changes, and fault events [27], [28]).

The inverter-based microgrid model is created for MATLAB/Simulink simulation in order to investigate the stability of the suggested technique during transient conditions. The system characteristics are provided in Table I, and Fig. 6 illustrates the configuration. It should be noted that the disturbance used in this investigation is the grid phase disturbance, as defined in [27], in order to immediately establish the power angle after the disturbance, which is useful for the quantitative study of the stability.

Fig. 4 displays the simulation results under various disturbances: (a) small disturbance; (b) large disturbance; (c) fault disturbance; (d) grid transition disturbance. The term "Proposed" in Fig. 4 refers to the virtual impedance based on FFNN. The system maintains stability and returns to equilibrium because, as illustrated in Fig. 4(a), the power angle of the proposed method following a small disturbance (small load switching) is still contained within the stability limit, as well as without virtual impedance but with slight oscillation. As seen in Fig. 4(b), after the system experiences a large disturbance (huge load switching), the power angle oscillation equals for the proposed method, while it is without virtual impedance, and the system continues to be stable in both methods. As seen in Fig. 4(c), when the system faces a significant disturbance (3-phase fault disturbance), the severe oscillation process causes to surpass the maximal stability limit, which ultimately results in instability when the system operates without virtual impedance also under the conventional virtual impedance, Fig. 14 in [26]. While using the proposed virtual impedance method, the system continues to be stable, and the power angle varies in the range of . As presented in Fig. 4(d), under grid transition disturbance, the proposed method shows a tiny change. In contrast, a continuous oscillation of at angular velocity clearly appears at the grid transition state because of the total equivalent impedance variation at the inverter tie-in point.

V. PHIL Experimental Verification

A. PHIL Experimental Setup

To assure the efficiency of the FFNN virtual impedance technology, experimental validations are conducted on a PHIL system. LabVolt three-phase inverters, DC power supplies, and real-time simulator make up the PHIL system, as illustrated in Fig 5. The Artemis library and MATLAB SimPowerSystems are used to create the microgrid, power circuit, loads, and LCL filter. Since the entire system comprises too many switches, the state-space nodal technique is required to delink the power circuit modeling, [29].

Applying a processing time-step of 100 , the described control scheme—which includes the FFNN—is constructed on a high-performance real-time architecture. Opal-RT Technologies' RT-EVENT library block, [30], is used to produce the driving pulses, which have a switching frequency of 2.7 . It's because the VSI gates' inputs are interfaced with the simulator's digital outputs. Using the analog input of the , the inverter's output voltage is instantly sensed. The DC voltage power source and voltage source inverters, scaled to /1MW, make up the actual BESSs. In Table I, the LCL filter's parameters and power system's parameters are listed.

Fig. 5. PHIL Experimental setup [24].

TABLE I
POWER SYSTEM PARAMETERS [24]

Parameter	Value
DC Voltage (V)	$v_{dc} = 922$
Nominal grid/load frequency (Hz)	$f = 60$
Nominal grid/load L-L voltage (V)	$v_{rms} = 600$
Inverter-side filter (mH, Ω)	$L_s = 0.7$, $R_s = 2.63 \cdot 10^{-4}$
Parallel filter (kVAr)	$Q_{C_f} = 50$
Grid-side filter (H, Ω)	$L_g = 0.06$, $R_g = 0.003$

B. Microgrid Testing model

The testing system is developed to cover the majority of operating scenarios and demonstrate the efficacy, robustness, and usefulness of the suggested approach since it is intended to be a universal FFNN virtual impedance bi-directional inverter-based microgrid droop controller. Fig. 6 demonstrates the testing scheme, which has a 1MW voltage source system. On the DC side, it is coupled to a battery storage system, and on the AC side, it is connected to an LCL filter and isolation transformer.

Fig. 6. Microgrid testing scheme.

Fig. 7 presents the PHIL experimental results for 1MW BESS for the proposed FFNN virtual impedance in comparison with the conventional VI and without VI as well. To evaluate that in both operating modes, grid-connected and

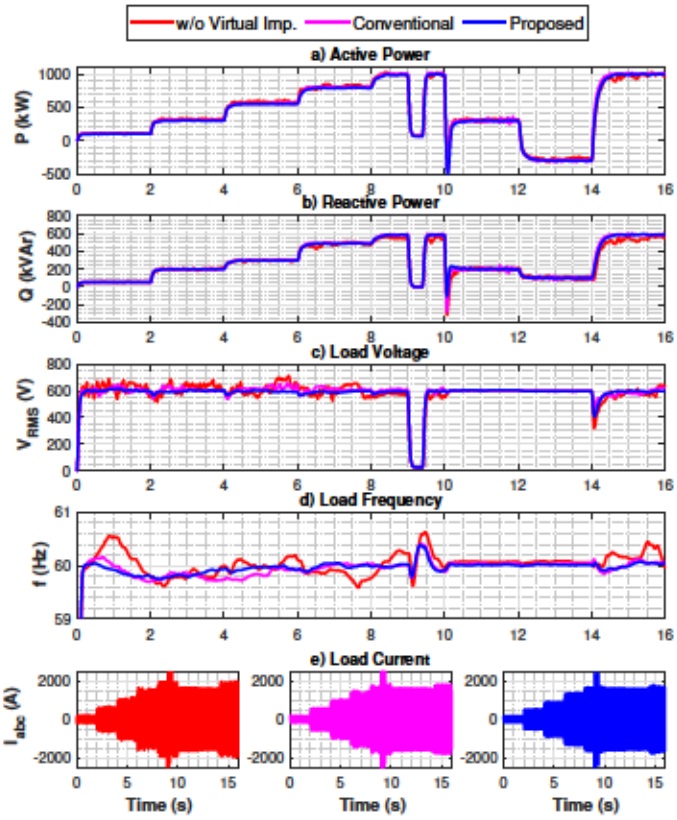

Fig. 7. PHIL experimental results for 1MW BESS.

islanded modes, a variant load and grid model are linked on the common busbar. Therefore, the 1MW BESS is tested in this section under:

1) Islanded Mode: The variant load power is changed in five steps, 100/50, 300/200, 550/300, 800/500, and 1000/600 kW/kVAr as illustrated in Fig. 7(a), (b) between 0 9 *sec.* From Active and reactive power curves, both the proposed and conventional methods deliver stable load power. While without virtual impedance, the delivered active and reactive load power fluctuate more at a high load level than at low power. Similar reactions are reflected on load current curves, Fig. 7(e), for the three presented methods.

The load voltage and frequency curves, Fig. 7(c), (d) and zoom-in scopes Fig. 8, demonstrate how far the proposed and conventional methods supply the required active and reactive power at the nominal voltage and frequency within an acceptable variation range. On the contrary, neglecting the

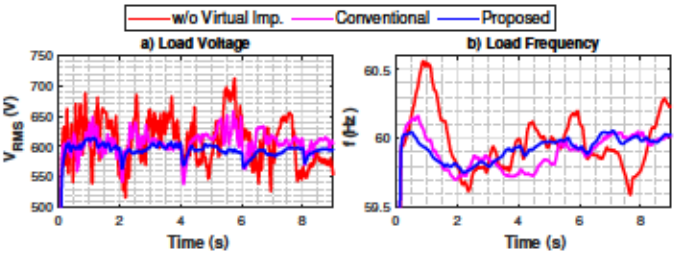

Fig. 8. Detail voltage and frequency results for 1MW BESS at islanded mode.

virtual impedance, the load voltage goes over the nominal voltage by 15%, Fig. 8(a), and the load frequency changes in the range of 1 Hz, but it exceeds the nominal frequency by 0.5 Hz.

2) Fault Dynamic Phase: A 3-phase fault is also applied during this phase at 9 *sec* for 0.4 *sec* to test the proposed method's dynamics during a significant disturbance. Fig. 9 focuses on the transient state of the active and reactive power, load voltage, and frequency. Fig. 9 confirms the capability of the proposed and conventional methods to supply the load power back after releasing the fault. Nevertheless, dropping the virtual impedance leads to a voltage drop and frequency swing out of the acceptable range during and after the fault.

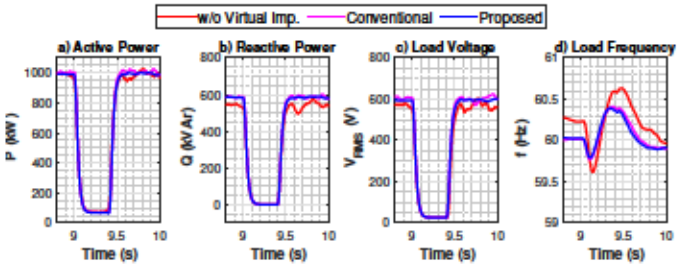

Fig. 9. PHIL experimental results for 1MW BESS at fault dynamic.

3) Islanded-Grid-Islanded Transition Mode: The transition from islanded to grid-connected mode is investigated during this phase. The VSI is operated in parallel with a swing bus, and the BESS shares the load per the reference active and reactive power values. The load power is held at 1000/600 kW/kVAr while the BESS's reference power values are modified to 300/200 and -300/100 kW/kVAr. The BESS serves as a load and charges the battery when the active power is negative, Fig. 7 between 10 14 *sec*. Back to islanded mode at 14 *sec*, the grid is switched off, and the BESS supplies the load at a value of 1000/600 kW/kVAr. Even more, at the transition points 10 *sec* and 14 *sec*, the suggested approach produces less load voltage fluctuation than the conventional method, Fig. 10(a); while the load frequency is almost the same in both methods, Fig. 10(b). On the other hand, the dynamic transition effect clearly appears in operating without virtual impedance rather than in the other methods because it does not match the grid-side impedance. To improve the accuracy of the active and reactive power sharing and reduce the circulating current during the transient state, this impedance must be changed. Consequently, the virtual impedance technique is the approach by which the dynamic transition states may be avoided [16].

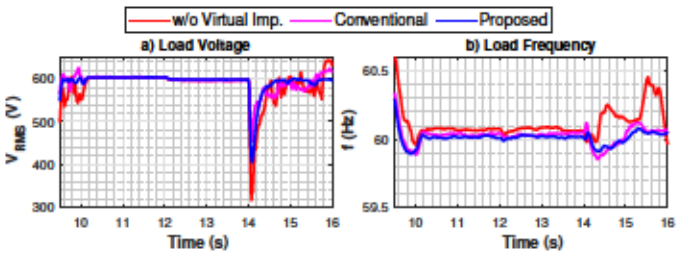

Fig. 10. Detail voltage and frequency results at transition mode.

Otherwise, during the steady-state period of grid-connected mode, the load voltage and frequency stick to the grid values.

Besides, in the proposed FFNN and conventional virtual impedance methods, the additional voltage values play the main part in system stability throughout transient states, with the system parameters' limitations, K_p, K_i, or $\hat{w}_{fi}^{(h)}$. At some points in the transitions and islanded/grid-connected modes, the conventional method cannot sustain the nominal system values, frequency and voltage tracking. Consequently, the suggested FFNN method demonstrates enhanced resilience to transient dynamics and variations in reference/load power. Variations in grid or load impedance produce rapid variations in v_{dq}^{+} voltages. The suggested approach can react quickly to sudden changes in the power flow, operating mode, or overall equivalent impedance. This solution has the advantage of a uniform and quick dynamical reaction since it employs a live weight adaptation approach over the v_{dq}^{+} voltages. The suggested approach is general and adaptable to each and every BESS size, with no more adjustment/tuning needed since it uses a per-unit base.

VI. IEEE 33-BUS STANDARD DISTRIBUTION SYSTEM

The proposed FFNN virtual impedance method is also confirmed within the standard IEEE 33-bus microgrid by connecting four inverters at different locations.

Fig. 11. IEEE 33-bus PHIL Experimental setup.

Case 1 : *Ring microgrid model* :
Fig. 11 and Fig. 12 present the standard IEEE 33-bus PHIL experimental setup and single line diagram, respectively, as proposed by [31] in a ring model (tie lines 33, 34, 35, 36, and 37 are in-service); in addition, it is integrated with four BESSs, 1 MW each. This test scenario verifies the FFNN method's robustness in generic grid/microgrid applications, whatever the installation location or total equivalent impedance at tie-in points. The test procedure is divided into two stages. The first one, Fig. 13, offers the normal operation stage at which each BESS operates in grid-connected mode at the reference active and reactive power, Table II and Fig. 13(a), (b). The proposed method achieves stable voltage at each

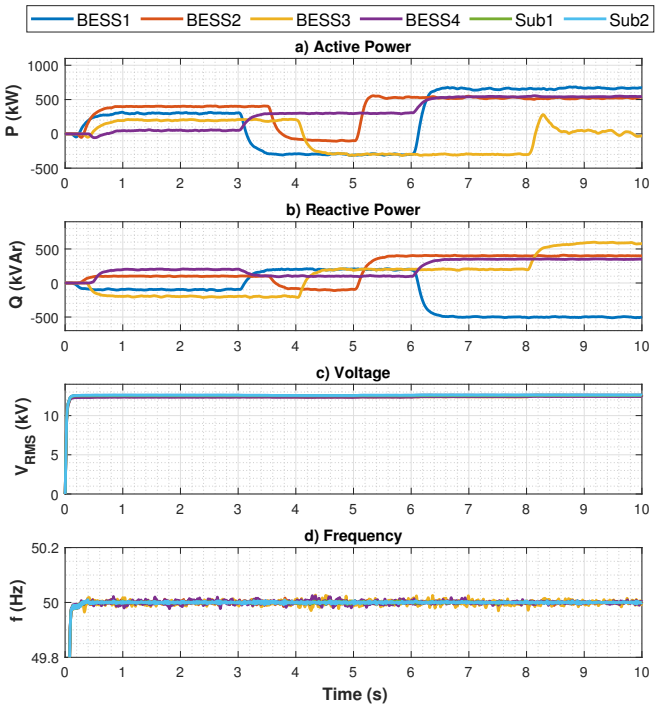

Fig. 13. PHIL experimental results for IEEE 33-bus ring microgrid integrated by four BESSs at normal operation.

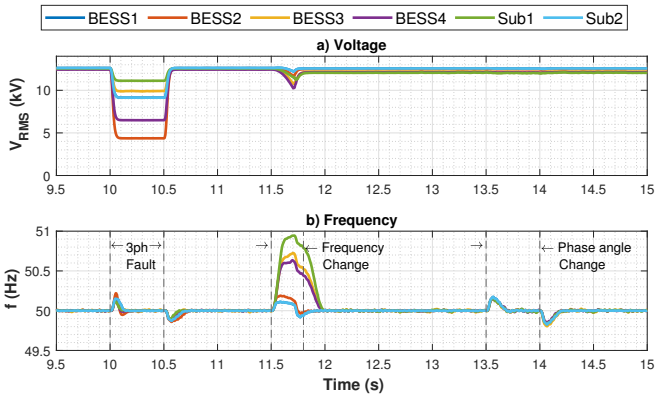

Fig. 14. PHIL experimental results for IEEE 33-bus ring microgrid integrated by four BESSs at dynamic operation.

Fig. 12. IEEE 33-bus single line diagram.

inverter's connection busbar (Fig. 13(c)) while ignoring frequency variations (Fig. 13(d)).

TABLE II
REFERENCE ACTIVE AND REACTIVE POWER

BESS1	BESS2	BESS3	BESS4	
0 - 3	0 - 3.5	0 - 4	0 - 3	sec
300 / -100	400 / 100	200 / -200	50 / 200	kW / kVAr
3 - 6	3.5 - 5	4 - 8	3 - 6	sec
-300 / 200	-100 / -100	-300 / 200	300 / 100	kW / kVAr
6 - 10	5 - 10	8 - 10	6 - 10	sec
650 / -500	550 / 400	50 / 600	550 / 350	kW / kVAr

In the second stage (Fig. 14), the dynamic transient operation is divided into three phases, i) At 10 sec, a 3-phase fault is applied and released at 10.5 sec. ii) At 11.5 sec, the first substation's (Sub1) frequency is changed by 1 Hz before the protection system takes action and trips this feeder at 11.7 sec. iii) At 13.5 sec, the second substation's phase angle is modified by 10 degrees before being adjusted back to the normal phase angle at 14 sec. Fig. 14(a), (b), voltage and frequency curves, confirm the proposed FFNN virtual impedance stability advantages by keeping each independent system stable during and after releasing the disturbances. On the contrary, the proposed method shows some acceptable deviation (close to 0.5 Hz) during high-impedance change, BESS3 and BESS4 during Sub1 frequency change. As BESS3 and BESS4 are closer to the disturbance source. Besides, the conventional virtual impedance method was also tested under the same operating conditions and gave the same results. They are not presented, however, because it is already confirmed in Section IV.

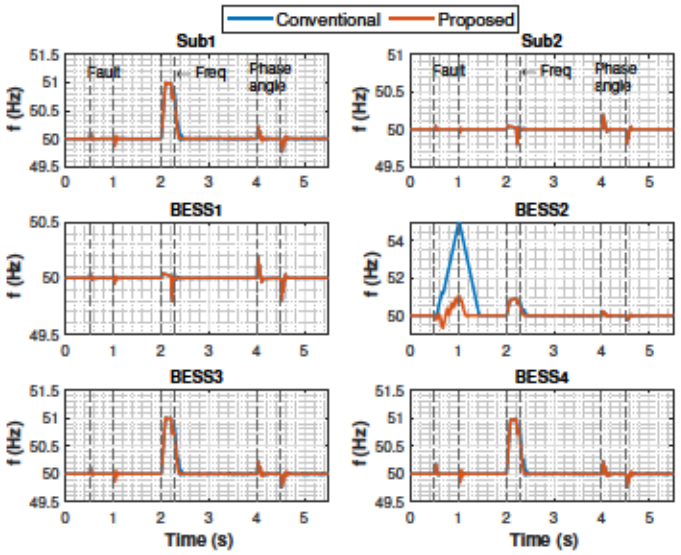

Fig. 15. IEEE 33-bus radial microgrid integrated by four BESSs at dynamic operation.

In this case, tie lines 33, 34, 35, 36, and 37 are out of service, and the above dynamic transient applications are conducted. Fig. 15 demonstrates the robustness of the proposed method against the conventional method. During this test, the PI controller of BESS2 cannot compensate for the highly nonlinear system. Therefore, the conventional system encounters unstable operating conditions. On the other hand, the proposed FFNN virtual impedance technique can keep the systems stable under significant disturbances. Thanks to the online weights adaptation method and FFNN structure that deal with nonlinear systems and can adjust the inverter terminal voltage (grid linkage impedance) to deliver the assigned power and keep the output frequency in the stability range.

VII. Conclusion

For bi-directional inverter-based microgrids, a control technique using feed-forward neural network virtual impedance is developed. A multi-layer feed-forward neural network trained using the back-propagation method with online weight modification is used to build a robust control method that improves stability during the dynamic operation. The FFNN has one hidden layer of ten neurons behind two neurons in the output layer. Additionally, the mathematical analysis of the microgrid droop control technique and FFNN structure serve as a foundation for the suggested technique. Combining these two approaches guarantees that distributed generation systems, such as BESSs, supply the grid or loads with the required energy. As a result, the load receives the demanded active and reactive power, maintaining the voltage and frequency of the system in islanded mode. Under grid-connected mode, the reference active and reactive power is maintained at the nominal system's voltage and frequency. Moreover, the proposed method is adapted to operate various VSI systems without any additional adjustment. Using real-time PHIL experimental studies, the effectiveness of the suggested procedure is examined throughout many phases. Simulink real-time software and an Opal-RT platform are used to build the PHIL setup. In order to test the 1MW BESS, the inverter bridge is driven by the system. Also, the IEEE 33-bus standard distribution system is tested in various scenarios assisted with four BESSs, that are based on the FFNN virtual impedance technique. In the highly nonlinear system, the conventional method cannot beat the proposed one, while the proposed FFNN virtual impedance technique can maintain system stability under significant disturbances. The neural network's offline training adds extra value because it minimizes the massive computational load associated with such traditional approaches. This, together with the live neuron-weight modification strategy, ensures stable performance. Finally, the experimental outcomes show how successful the suggested control technique is in both running modes. Otherwise, the proposed method shows some deviation during high-impedance change. Thus, future work will investigate and analyze this state performance and improvement for the FFNN control technique and avoid these deviations.

References

[1] S. Parhizi, H. Lotfi, A. Khodaei, and S. Bahramirad, "State of the Art in Research on Microgrids: A Review," *IEEE Access*, vol. 3, pp. 890–925, 2015.

[2] M. H. Saeed, W. Fangzong, B. A. Kalwar, and S. Iqbal, "A Review on Microgrids' Challenges & Perspectives," *IEEE Access*, vol. 9, pp. 166 502–166 517, 2021.

[3] D. E. Olivares, A. Mehrizi-Sani, A. H. Etemadi, C. A. Cañizares, R. Iravani, M. Kazerani, A. H. Hajimiragha, O. Gomis-Bellmunt, M. Saeedifard, R. Palma-Behnke, G. A. Jiménez-Estévez, and N. D. Hatziargyriou, "Trends in Microgrid Control," *IEEE Transactions on Smart Grid*, vol. 5, no. 4, pp. 1905–1919, July 2014.

[4] D. Yan and Y. Chen, "Distributed Coordination of Charging Stations with Shared Energy Storage in a Distribution Network," *IEEE Transactions on Smart Grid*, pp. 1–1, 2023.

[5] J. M. Guerrero, J. C. Vasquez, J. Matas, L. G. de Vicuna, and M. Castilla, "Hierarchical Control of Droop-Controlled AC and DC Microgrids—A General Approach Toward Standardization," *IEEE Transactions on Industrial Electronics*, vol. 58, no. 1, pp. 158–172, Jan. 2011.

[6] J. Hu, Y. Shan, K. W. Cheng, and S. Islam, "Overview of Power Converter Control in Microgrids—Challenges, Advances, and Future Trends," *IEEE Transactions on Power Electronics*, vol. 37, no. 8, pp. 9907–9922, Aug. 2022.

[7] J. Rocabert, A. Luna, F. Blaabjerg, and P. Rodríguez, "Control of Power Converters in AC Microgrids," *IEEE Transactions on Power Electronics*, vol. 27, no. 11, pp. 4734–4749, Nov. 2012.

[8] A. Gupta, S. Doolla, and K. Chatterjee, "Hybrid AC–DC Microgrid: Systematic Evaluation of Control Strategies," *IEEE Transactions on Smart Grid*, vol. 9, no. 4, pp. 3830–3843, July 2018.

[9] E. Espina, J. Llanos, C. Burgos-Mellado, R. Cárdenas-Dobson, M. Martínez-Gómez, and D. Sáez, "Distributed Control Strategies for Microgrids: An Overview," *IEEE Access*, vol. 8, pp. 193 412–193 448, 2020.

[10] J. Li, Q. Luo, D. Mou, Y. Wei, P. Sun, X. Du, and M. Liserre, "Energy Optimization Management Strategy for DC Nano-Grid Cluster with High Comprehensive Energy Efficiency," *IEEE Transactions on Smart Grid*, pp. 1–1, 2023.

[11] H. Safamehr, I. Izadi, and J. Ghaisari, "Robust V-I Droop Control of Grid-forming Inverters in the Presence of Feeder Impedance Variations & Nonlinear Loads," *IEEE Transactions on Industrial Electronics*, pp. 1–9, 2023.

[12] J. Schiffer, T. Seel, J. Raisch, and T. Sezi, "Voltage Stability and Reactive Power Sharing in Inverter-Based Microgrids With Consensus-Based Distributed Voltage Control," *IEEE Transactions on Control Systems Technology*, vol. 24, no. 1, pp. 96–109, Jan. 2016.

[13] A. Firdaus and S. Mishra, "Mitigation of Power and Frequency Instability to Improve Load Sharing Among Distributed Inverters in Microgrid Systems," *IEEE Systems Journal*, vol. 14, no. 1, pp. 1024–1033, March 2020.

[14] M.-D. Pham and H.-H. Lee, "Effective Coordinated Virtual Impedance Control for Accurate Power Sharing in Islanded Microgrid," *IEEE Transactions on Industrial Electronics*, vol. 68, no. 3, pp. 2279–2288, March 2021.

[15] N. Mohammed, A. Lashab, M. Ciobotaru, and J. M. Guerrero, "Accurate Reactive Power Sharing Strategy for Droop-based Islanded AC Microgrids," *IEEE Transactions on Industrial Electronics*, vol. 70, no. 3, pp. 2696–2707, March 2023.

[16] M. Ahmed, L. Meegahapola, A. Vahidnia, and M. Datta, "Adaptive Virtual Impedance Controller for Parallel and Radial Microgrids With Varying X/R Ratios," *IEEE Transactions on Sustainable Energy*, vol. 13, no. 2, pp. 830–843, April 2022.

[17] H. K. Morales-Paredes, D. Tardivo, C. D. Burgos Mellado, and J. P. Bonaldo, "Enhanced Control Strategy based on Virtual Impedance Loops to Achieve the Sharing of Imbalance and Harmonic in 3-Phase 4-Wire Isolated Microgrids," *IEEE Transactions on Power Delivery*, vol. 37, no. 4, pp. 3412–3415, Aug. 2022.

[18] B. Fan, Q. Li, W. Wang, G. Yao, H. Ma, X.-j. Zeng, and J. M. Guerrero, "A Novel Droop Control Strategy of Reactive Power Sharing Based on Adaptive Virtual Impedance in Microgrids," *IEEE Transactions on Industrial Electronics*, vol. 69, no. 11, pp. 11 335–11 347, Nov. 2021.

[19] F. Luo, Y. Chen, Z. Xu, G. Liang, Y. Zheng, and J. Qiu, "Multiagent-Based Cooperative Control Framework for Microgrids' Energy Imbalance," *IEEE Transactions on Industrial Informatics*, vol. 13, no. 3, pp. 1046–1056, June 2017.

[20] A. C R and U. B. Manthati, "A Hybrid Controller Assisted Voltage Regulation and Power Splitting Strategy for Battery/ Supercapacitor System in Isolated DC Microgrid," *IEEE Transactions on Energy Conversion*, pp. 1–10, 2023.

[21] P. Liu, Y. Bi, and C. Liu, "Data-Based Intelligent Frequency Control of VSG via Adaptive Virtual Inertia Emulation," *IEEE Systems Journal*, vol. 16, no. 3, pp. 3917–3926, Sept. 2022.

[22] D.-D. Zheng, S. S. Madani, and A. Karimi, "Data-Driven Distributed Online Learning Control for Islanded Microgrids," *IEEE Journal on Emerging and Selected Topics in Circuits and Systems*, vol. 12, no. 1, pp. 194–204, March 2022.

[23] H. R. Baghaee, M. Mirsalim, and G. B. Gharehpetian, "Power Calculation Using RBF Neural Networks to Improve Power Sharing of Hierarchical Control Scheme in Multi-DER Microgrids," *IEEE Journal of Emerging and Selected Topics in Power Electronics*, vol. 4, no. 4, pp. 1217–1225, Dec. 2016.

[24] M. Alzayed, M. Lemaire, S. Zarrabian, H. Chaoui, and D. Massicotte, "Droop-controlled bidirectional inverter-based microgrid using cascade-forward neural networks," *IEEE Open Journal of Circuits and Systems*, vol. 3, pp. 298–308, 2022.

[25] M. Alzayed, H. Chaoui, and Y. Farajpour, "Maximum Power Tracking for a Wind Energy Conversion System Using Cascade-Forward Neural Networks," *IEEE Transactions on Sustainable Energy*, vol. 12, no. 4, pp. 2367–2377, Oct. 2021.

[26] Y. Tang, Z. Tian, X. Zha, X. Li, M. Huang, and J. Sun, "An Improved Equal Area Criterion for Transient Stability Analysis of Converter-Based Microgrid Considering Nonlinear Damping Effect," *IEEE Transactions on Power Electronics*, vol. 37, no. 9, pp. 11 272–11 284, Sept. 2022.

[27] Y. Liu, M. Huang, C. K. Tse, H. H.-C. Iu, Z. Yan, and X. Zha, "Stability and Multiconstraint Operating Region of Grid-Connected Modular Multilevel Converter Under Grid Phase Disturbance," *IEEE Transactions on Power Electronics*, vol. 36, no. 11, pp. 12 551–12 564, Nov. 2021.

[28] M. G. Taul, X. Wang, P. Davari, and F. Blaabjerg, "Robust Fault Ride Through of Converter-Based Generation During Severe Faults With Phase Jumps," *IEEE Transactions on Industry Applications*, vol. 56, no. 1, pp. 570–583, Jan.-Feb. 2020.

[29] C. Dufour, J. Mahseredjian, and J. Bélanger, "A Combined State-Space Nodal Method for the Simulation of Power System Transients," *IEEE Transactions on Power Delivery*, vol. 26, no. 2, pp. 928–935, April 2011.

[30] C. Rabbath, M. Abdoune, and J. Belanger, "Effective real-time simulations of event-based systems," in *2000 Winter Simulation Conference Proceedings (Cat. No.00CH37165)*, vol. 1, 2000, pp. 232–238 vol.1.

[31] M. Baran and F. Wu, "Network reconfiguration in distribution systems for loss reduction and load balancing," *IEEE Transactions on Power Delivery*, vol. 4, no. 2, pp. 1401–1407, April 1989.

Mohamad Alzayed (M'20) received the Ph.D. degree in Electrical and Computer Engineering from Carleton University, Ottawa, ON, Canada. His career has bridged both academia and industry with more than 14 years of experience in control and electrical energy resources, grid management and efficiency, electrical design and contracting, and project management. Since 2019, he has been a member of the Intelligent Robotic and Energy Systems (IRES) research group, Department of Electronics, Carleton University, and joined the Laboratory of Signal and System Integration (LSSI), Department of Electrical and Computer Engineering, the University of Quebec at Trois-Rivières, in 2022. His teaching/research activities focus on intelligent control of electric machines and power converters for energy systems, real-time simulations, and power systems. He is a member of IEEE and a Guest Editor of several journals.

Michel Lemaire received his M.S. and B.S. degrees in Electrical Engineering from the University of Quebec, Trois-Rivières (UQTR), department of Electrical Engineering, QC, Canada, in 2014 and 2017, respectively. He obtained his Ph.D. in Electrical Engineering from UQTR in 2024, with a thesis focusing on the FPGA implementation of electric circuit solvers for real-time applications. He is currently serving as a post-doctoral researcher at the LSSI lab at UQTR. His research interests encompass Power Hardware-In-the-Loop (PHIL) and Hardware-In-the-Loop (HIL) simulation systems, real-time simulation, electric circuit modeling and solving, control and power electronics, motor and grid emulation, four-quadrant amplifier design, and low-latency inter-FPGA communication.

Hicham Chaoui (S'01-M'12-SM'13) received the Ph.D. degree in electrical engineering from the University of Quebec, Trois-Rivières, QC, Canada, in 2011. His career has spanned both academia and industry in the field of control and energy systems. From 2007 to 2014, he held various engineering and management positions with Canadian industry. He is currently an Associate Professor at Carleton University, Ottawa, ON, Canada. His scholarly work has resulted in more than 200 journal and conference publications. He is a Registered Professional Engineer in the province of Ontario and an Associate Editor of several IEEE journals. He was the recipient of the Best Thesis Award, the Governor General of Canada Gold Medal Award, the Carleton's Research Excellence Award, the Early Researcher Award from the Ministry of Colleges and Universities, and the Top Editor Recognition from IEEE Vehicular Technology Society.

Daniel Massicotte (S'91–M'94–SM'08) received the B.Sc.A. and M.Sc.A. degrees in electrical engineering and industrial electronics in 1987 and 1990 respectively from the Université du Québec à Trois-Rivières (UQTR), Qc, Canada. He obtained the Ph.D. degree in electrical engineering in 1995 at the École Polytechnique de Montréal, Qc, Canada. In 1994, he joined the Department of Electrical and Computer Engineering, Université du Québec à Trois-Rivières, where he is currently a Full Professor. He is Founder of the Laboratory of Signal and Systems Integration. Since 2001, he has been Founding President and Chief Technology Officer of Axiocom Inc. He has been Head of the Industrial Electronic Research Group from 2011 to 2018 and Head of the Electrical and Computer Engineering Department, since 2014. Head of the Research Chair in Signals and Intelligence of High-Performance Systems. He received the Douglas R. Colton Medal for Research Excellence awarded by the Canadian Microelectronics Corporation, the PMC-Sierra High Speed Networking and Communication Award and the Second place at the Complex Multimedia/Telecom IP Design Contest from Europractice. His research interests include advanced VLSI implementation, digital signal processing for wireless communications, measurement, medical, real-time simulation and control problems for linear/nonlinear complex systems. He has proposed many methods based on modern signal processing, such as machine learning, transform domain, and metaheuristics. He is author/coauthor of more than 200 technical papers in international conferences and journals, as well as of 9 inventions. Dr. Massicotte is also member of the "Ordre des Ingénieurs du Québec" and "Microsystems Strategic Alliance of Quebec" (ReSMiQ).